POSITRON SOURCES

R. Chehab

Laboratoire de l'Accélérateur Linéaire, IN2P3-CNRS
et Université de Paris-Sud, 91405 Orsay Cedex, France

Abstract

A tentative survey of positron sources is given. Physical processes on which positron generation is based are indicated and analyzed. Explanation of the general features of electromagnetic interactions and nuclear β^+ decay makes it possible to predict the yield and emittance for a given optical matching system between the positron source and the accelerator. Some kinds of matching systems commonly used – mainly working with solenoidal field – are studied and the acceptance volume calculated. Such knowledge is helpful in comparing different matching systems. Since for large machines, a significant distance exists between the positron source and the experimental facility, positron emittance has to be preserved during beam transfer over large distances and methods used for that purpose are indicated. Comparison of existing positron sources leads to extrapolation to sources for future linear colliders. Some new ideas associated with these sources are also presented.

INTRODUCTION

In recent years, there has been increasing interest in the use of high intensity positron beams in storage and collider rings. With the advent of linear colliders such as SLC or others presently under study, more stringent conditions are imposed on positron intensity and emittance.

Positron beam intensity and emittance are strongly related to the methods of production and collection. Positron generation by electromagnetic interaction or nuclear β^+ decay present different features which will be analyzed. Thermic processes in the target have also to be considered. However, knowledge of the positron production rate is insufficient to calculate the actual beam intensity which is also dependent on collection devices and, obviously, on linac acceptance. Positron emittance is mainly determined by the converter and the matching system. Very often, longitudinal ($\Delta\emptyset$, $\Delta E/E$) and transverse (x,x'; y, y') emittances have to be reduced to deal with storage ring injection requirements or linear collider interaction point conditions. Beam transport and trajectory control are of particular importance in ensuring that the intensity and emittance of the beam are protected from the effects of wakefields. Some comparisons between existing e^+ sources will lead to predictions of yields, emittance and the feasibility of positron sources for linear colliders.

1. PHYSICAL PROCESSES ASSOCIATED WITH POSITRON PRODUCTION

Two kinds of physical processes are generally considered for positron production: the electromagnetic interaction of a photon with the Coulomb field of the nucleus with consequent pair production, and the weak interaction occuring in nuclear β^+ decay. Coherent pair production in a strong electromagnetic field using a very high energy electron beam could also be foreseen in some particular cases (cf. 2).

1.1 Electromagnetic interaction [1]

Charged particles traversing a target lose energy by radiation and collision. The energy lost by collision is used in atom excitation and ionization leading to secondary electron emission and is hence essentially dissipated. This represents the main contribution to heating processes in the target. The energy lost by radiation – Bremsstrahlung – is distributed among the secondary photons whose energy can reach the primary electron energy. The created photons interacting with the nucleus, and in a weaker manner with the peripheral electrons, undergo materialization with subsequent pair creation. The Compton effect could also occur by elastic collision of the photons with electrons. The electron pairs radiate photons and are then transformed into other pairs, the energy of the created electrons decreasing at each step. Such a process is called a cascade shower (Fig. 1). Electromagnetic showers can be initiated by high energy photons as well as by high energy electrons.

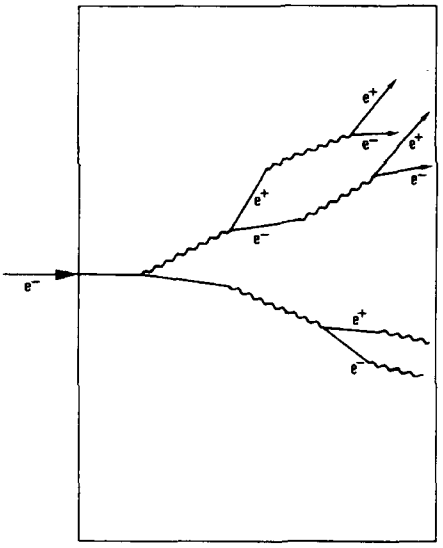

Fig. 1 Electron generated cascade shower

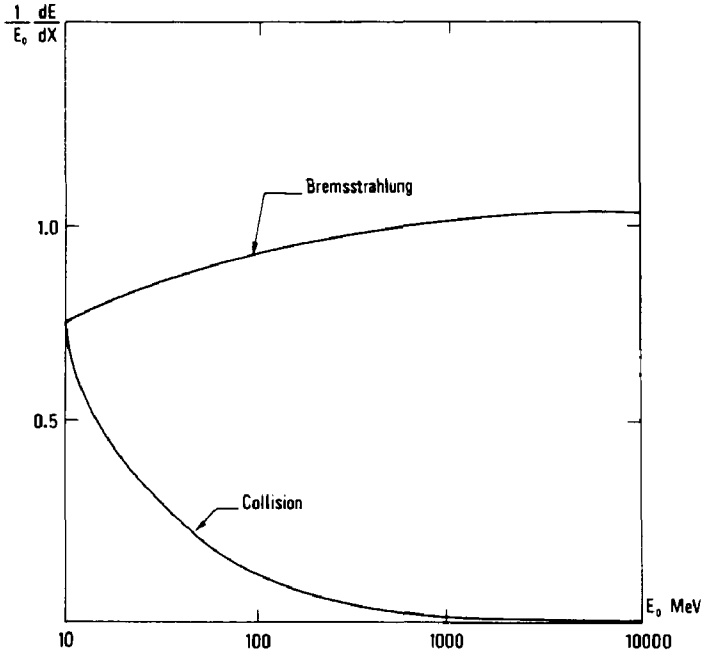

Fig. 2 Fractional energy losses by collision and Bremsstrahlung (from B. Rossi, Ref. [1])

Bremsstrahlung, pair creation, ionization and Compton effect are not the only processes encountered. Among others, multiple Coulomb scattering is of some importance since it mainly determines the lateral spread of the shower. The relative importance of these various phenomena may be examined by comparing their cross sections. We present in Fig. 2 the losses by Bremsstrahlung and collision processes. For positron production, pair materialization of photon – directly impinging on the target or radiated by the incident electrons – is the essential phenomenon. The Bremsstrahlung differential cross section is given by [2]:

$$\frac{d\sigma_{Brem}(Z,E_0,k)}{dk} = \frac{A(Z,E_0) r_e^2 \alpha Z (Z + \xi(Z))}{k}$$

$$x \left\{ (1 + (E/E_0)^2) \left[\phi_1(\delta) - \frac{4}{3} \ell n Z - (4 f_c(Z) \text{ if } E_0 > 50,0) \right] \right. \tag{1.1}$$

$$\left. - \frac{2}{3} (E/E_0) \left[\phi_2(\delta) - \frac{4}{3} \ell n Z - (4 f_c(Z) \text{ if } E_0 > 50,0) \right] \right\}$$

where E_0 is the incident electron energy in MeV

$\alpha = 1/137$
r_e, electron classical radius
k, photon energy in MeV
E, electron energy in MeV
Z, target material atomic number
$\delta = \frac{136}{Z^{1/3}} \frac{km}{E_0 E}$
$\varphi_1(\delta)$ and $\Phi_2(\delta)$ are the screening functions
$f_c(Z)$ is the Coulomb correction term (Davies, Bethe, Maximon)
m is the electron rest energy in MeV.

The pair production cross section is given by

$$\frac{d\sigma_{pair}(Z,k,E_+)}{dE_+} = \frac{A'_p(Z,k) r_e^2 \alpha Z (Z + \xi(Z))}{k^3}$$

$$x \left\{ (E_+^2 + E_-^2) \left[\phi_1(\delta) - \frac{4}{3} \ell n Z - (4 f_c(Z) \text{ if } k > 50,0) \right] \right. \tag{1.2}$$

$$\left. + \frac{2}{3} (E_+ E_-) \left[\phi_2(\delta) - \frac{4}{3} \ell n Z - (4 f_c(Z) \text{ if } k > 50,0) \right] \right\}$$

where E_+ and E_- are the positron and electron energies respectively

$\xi = \ln (1440 Z^{-2/3}) / \ln (183 Z^{-1/3})$
$\delta = \frac{136}{Z^{1/3}} \frac{km}{E_+ E_-}$

We may notice that Bremsstrahlung and pair production cross sections are a rapidly increasing function of the material's atomic number. For this reason tungsten (74) and tantalum (73) are good candidates for positron converters.

1.1.1 Some methods for shower analysis

Analytical as well as numerical analysis have been extensively used to study positron generation.

1.1.1.1 Analytical approaches

Since angles of emission of secondary electrons and photons at high energies are quite small in low Z elements, the electron scattering is also small and the electromagnetic cascade shower is developed in the direction of the incident particle. This allows the longitudinal shower development and the lateral spread to be treated as two separate problems. For higher Z materials this assumption remains valid only for the more energetic secondary particles. Nevertheless, it constitutes a convenient approach and the following approximations can be built on this basis:

A) considers only Bremsstrahlung and pair creation.
B) improves the former taking into account the ionization losses at a constant rate, and
C) uses more precise cross section evaluations regarding B and takes into account the Compton effect [1].

Two quantities are relevant to positron production in the longitudinal direction: the position of the shower maximum and the number of secondary particles (e^+ and e^-) at this maximum. Both are derived using approximation B.

The position of the shower maximum is given by [1]:

$$T^{e^-}_{max} = 1.01\left[\ell n\left(E_0/\varepsilon_0\right) - 1\right] \tag{1.3}$$

for a primary electron

where E_0 is the incident electron energy

ε_0 the material critical energy (energy at which radiation losses and collision losses are almost identical), and

$$T^{\gamma}_{max} = 1.01\left[\ell n\left(E_0/\varepsilon_0\right) - \frac{1}{2}\right] \tag{1.4}$$

for a primary photon.

The number of secondary particles at shower maximum is given by [1]:

$$\Pi^{e^-}_{max} = \frac{0.31}{\left[\ell n\left(E_0/\varepsilon_0\right) - 0.37\right]^{1/2}} \cdot \frac{E_0}{\varepsilon_0} \tag{1.5}$$

for a primary electron, and

$$\Pi^{\gamma}_{max} = \frac{0.31}{\left[\ell n\left(E_0/\varepsilon_0\right) - 0.18\right]^{1/2}} \cdot \frac{E_0}{\varepsilon_0} \tag{1.6}$$

for a primary photon.

These formulae clearly show the importance of using high energy incident particles. However, they give values which are too optimistic (see Figs. 3 and 4) compared with more exact calculations and especially the Monte Carlo simulations by Crawford and Messel [3,4].

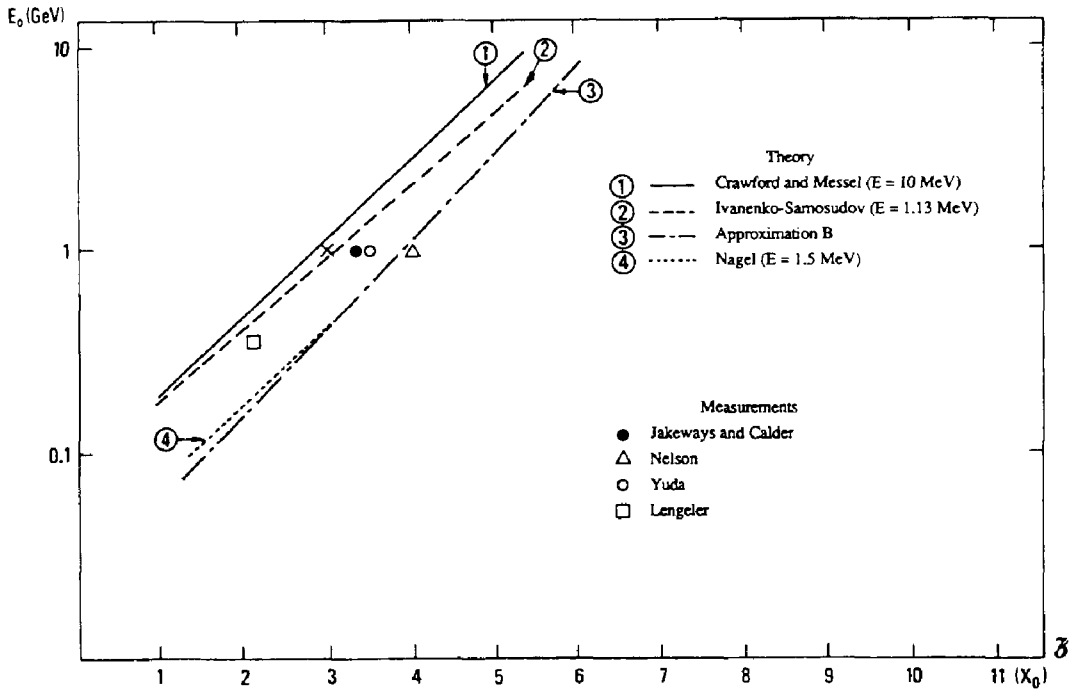

Fig. 3 Shower maximum position variation with incident energy (lead). Cut-off energy E is indicated (from R. Chehab, Ref. [4]).

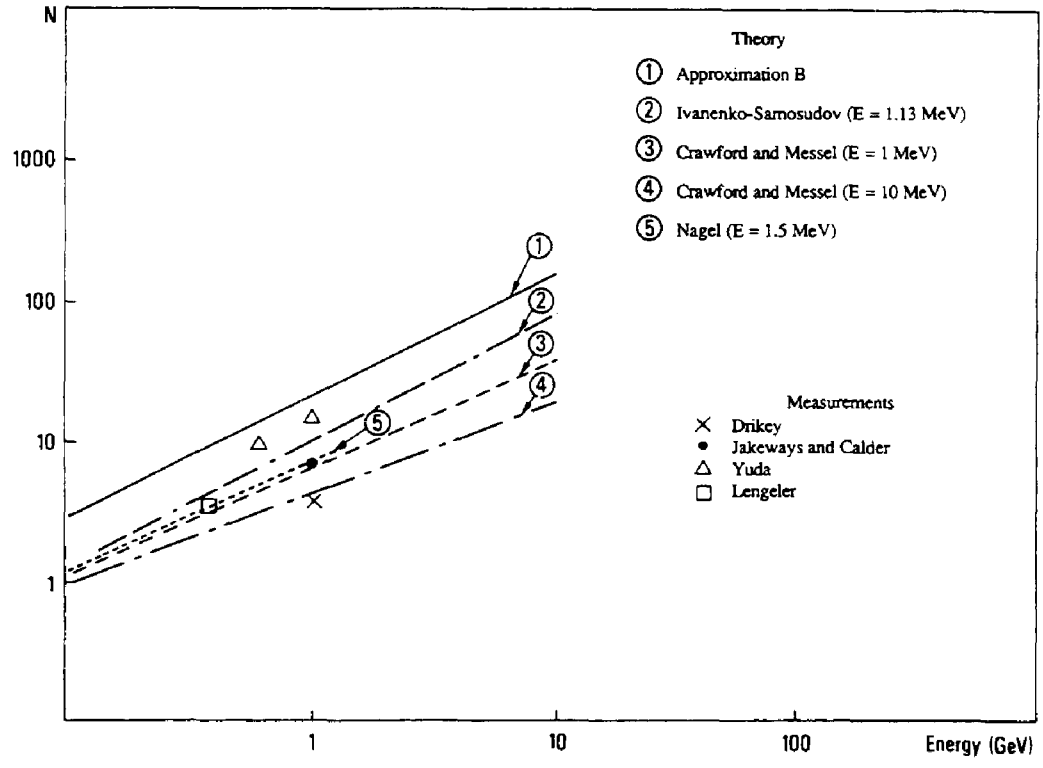

Fig. 4 Number of secondary particles at shower maximum (lead). Cut-off energy E is indicated (from R. Chehab, Ref. [4]).

Most of the lateral spread features are due to multiple scattering. If we consider a parallel and infinitely narrow beam of particles impinging on a thin plate – so as to neglect the

energy losses – we can describe the distribution of the secondary particles (in the y – θ_y plane) by the Fermi function [1]:

$$P(z,y\theta_y)\, d_y\, d\theta_y = \frac{2\sqrt{3}}{\pi} \cdot \frac{1}{\theta_s^2\, z^2} \exp\left\{ -\frac{4}{\theta_s^2}\left(\frac{\theta_y^2}{z} - \frac{3y\theta_y}{z^2} + \frac{3y^2}{z^3} \right) \right\} \qquad (1.7)$$

where $\theta^{2;s}$ represents the mean square angle of scattering defined by:

$$\theta_s = \frac{15}{E} \sqrt{\frac{z}{X_0}}$$

1.1.1.2 Monte Carlo simulation

When considering transport by magnetic lenses of positrons collected from the source, we are concerned with low energy positrons (some MeV). Moreover, use of high Z materials to improve pair creation leads to important electron scattering and hence to the lengthening of the particle path. Longitudinal development and lateral spread can no longer be separated. Monte Carlo calculations provide a more consistent approach to the problem due to more precise and complete analysis and from these Crawford and Messel tables [3] and EGS code [2] provide a good description of the problem. We shall use here mainly EGS results – and also GEANT [5] for some applications – for a positron source excited by an electron or a photon beam.

We may characterize a positron source by its density $d^3n/dE\, dr\, d\Omega$ where E, r and Ω represent respectively the energy, radial distance to the axis and solid angle of emission of the emitted positron. Such a density may be determined at the converter exit using EGS code. To calculate the optimum thickness of the converter, we make use of the "Transition curve" (Fig. 5) which gives the variation of the number of secondary particles with the penetration depth of the material.

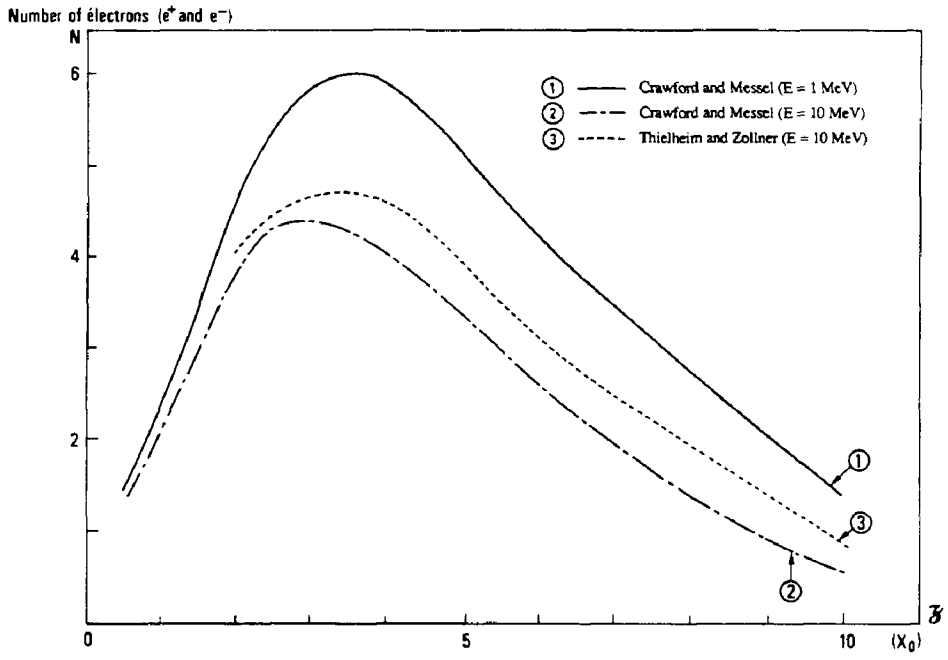

Fig. 5 Transition curve for 1 GeV incident electron (lead). Cut-off energy E is indicated (from R. Chehab, Ref. [4]).

Positron density and, more generally, positron emittance in the six-dimensional phase space [x, dx/dz; y, dy/dz; $\Delta\phi$, ΔE] may be represented – in a restrictive manner – by the following curves:

– Positron energy spectrum (Fig. 6)
– Radial distribution (Fig. 7)
– Angular distribution (Fig. 8).

Given an acceptance volume v defined by the limits:

$$[(E_{min}, E_{max}) ; r_{max} ; \theta_{max}]$$

we can write for the positron yield

$$n^{+} = n_0 \iiint_v \frac{d^3 n}{dE\, dr\, d\Omega}\, dE\, dr\, d\Omega \qquad (1.8)$$

where n_0 is the total number of positrons produced by one incident electron or photon and $d\Omega$ is the elementary solid angle defined by

$$d\Omega = 2\pi \sin\theta\, d\theta.$$

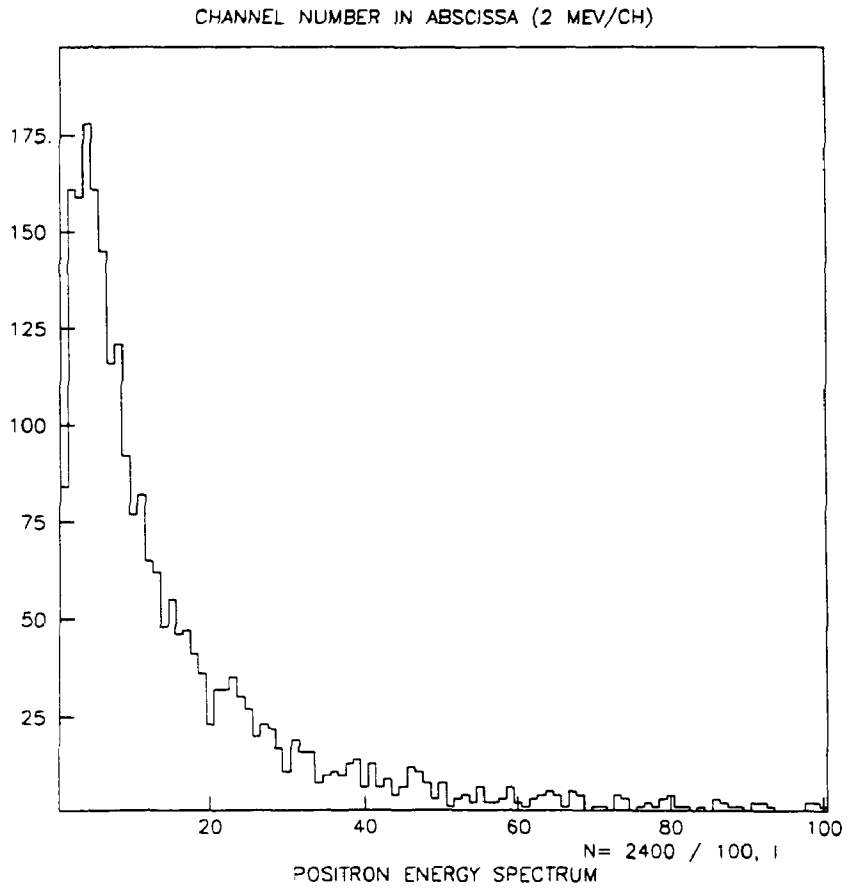

Fig. 6 Positron energy spectrum

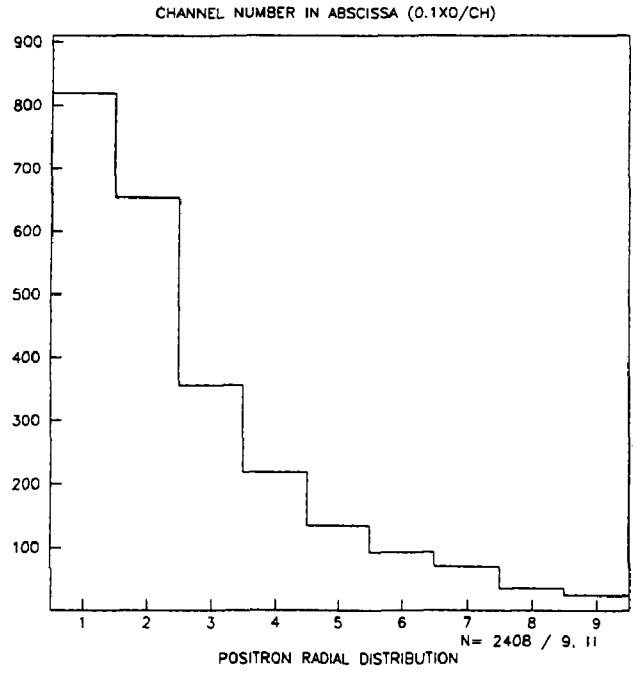

Fig. 7 Positron radial distribution

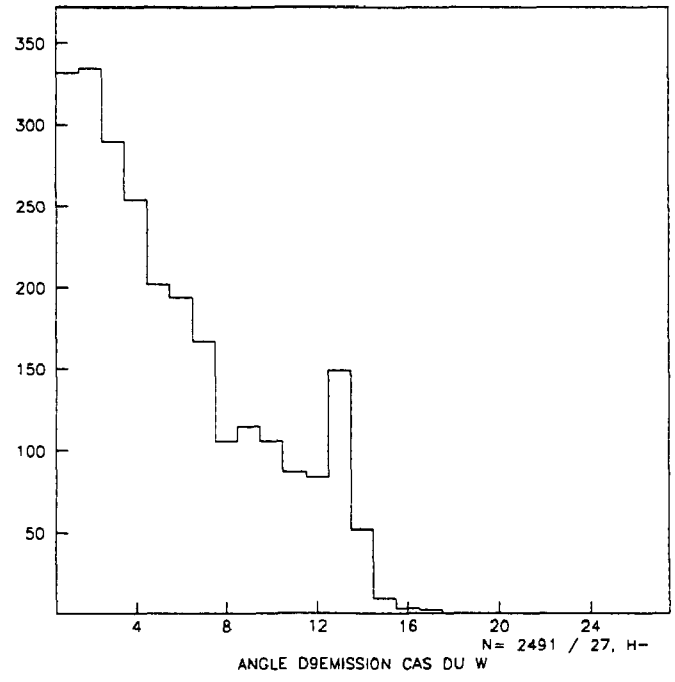

Fig. 8 Positron angular distribution

Such an expression can also be written as:

$$n^{+} = n_0 \int_{E_{min}}^{E_{max}} \int_{0}^{r_{max}} \int_{0}^{\theta_{max}} f_E(E)\, f_r(r,E)\, f_\theta(\theta,E)\, 2\pi \sin\theta \, d\theta \, dr \, dE \qquad (1.9)$$

where f_E, f_r, f_θ are the distribution functions which can be derived from EGS simulations.

Nota : A more appropriate calculation should take into account the distribution in transverse momentum – which can be derived from EGS – instead of the angular distribution.

1.1.2 Thermic processes and radiation problems

Energy losses by ionization lead to thermal heating of the target while photons as well as secondary particles (e^+ and e^-) created in the target and not collected by the optical system produce a large amount of radiation.

1.1.2.1 Thermal heating

The thermic behaviour of the converter depends upon the electron beam intensity, dimensions, pulse width and repetition rate as well as the physical properties of the material. A basic quantity is represented by the fractional energy absorption per cm^3: $1/E_0 \cdot dE(r,z)/dv$ which can be obtained from shower codes such as EGS. We can also use the energy deposition per unit lengh in the target: $1/E_0 \cdot dE/dz$ where E_0 is the incident electron energy. In Fig. 9, we show an example for this last quantity calculated for a tungsten target receiving a 2 GeV electron beam. We notice that most of the energy is deposited in the last fraction of the converter.

The pulse temperature rise is given by:

$$\Delta t_p = \frac{N E_0}{\rho C_p} \cdot \frac{1}{E_0} \cdot \frac{dE}{dv} \qquad (1.10)$$

where ρ is the material density

C_p its heat capacity
N is the number of particles per pulse.

For a given peak intensity, this quantity grows linearly with the pulse width and inversely as the square of the beam diameter.

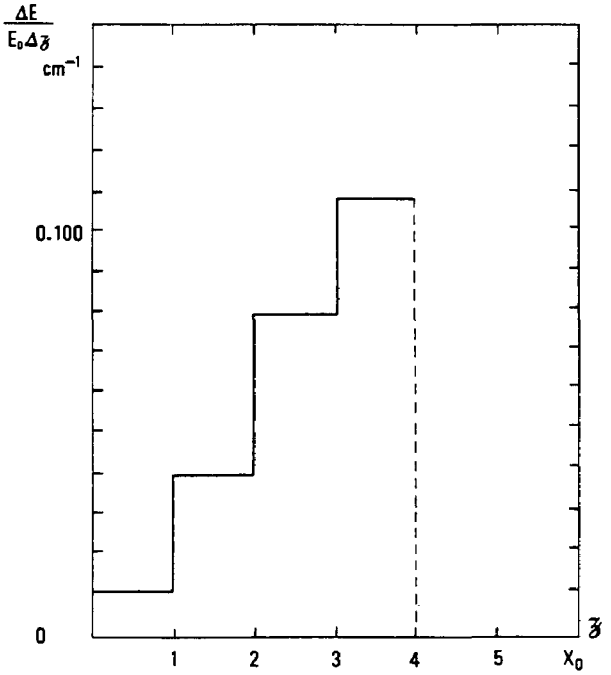

Fig. 9 Fractional energy absorption per unit length for 2 GeV electron

For a target of cylindrical geometry, the steady state temperature rise is given by [6]:

$$Q(r) = \nu N E_0 \int_0^r \frac{1}{E}\frac{dE}{dv} 2\pi r\, dr = k_t\, 2\pi r \frac{dT}{dr} \qquad (1.11)$$

where ν is the pulse repetition rate

k_t is the thermal conductivity.

$\frac{1}{E}\frac{dE}{dv}$ may be smoothed with a regular function and the expression (1.11) easily integrated.

Fatigue of the material may arise from stresses caused by thermal pulses. For a disk heated symmetrically about its centre, and uniformly throughout its thickness, the stresses are given as functions of the radius by [7]:

$$\sigma_{r_1} = \tau E_y \left(\frac{1}{R^2} \int_0^R T(r)\, r\, dr - \frac{1}{r_1^2} \int_0^{r_1} T(r)\, r\, dr \right)$$

$$\sigma_{z_1} = \tau E_y \left(-T(r) + \frac{1}{R^2} \int_0^R T(r)\, r\, dr + \frac{1}{r_1^2} \int_0^{r_1} T(r)\, r\, dr \right) \qquad (1.12)$$

where R is the disk radius

T(r) is the temperature at any point a distance r from the centre, minus the temperature of the coldest part of the disk

τ is the coefficient of thermal expansion

E_y is the Young modulus.

For T(r), we can take the pulse temperature rise Δt_p. In the expression (1.10), the quantity $1/E_0 \cdot dE/dv$ is a decreasing function of r and, therefore, also Δt_p. Thus the maximum stresses (at the hot central core) are given by:

$$\sigma_r = \sigma_z = -\frac{\tau E_y \Delta t_p(0)}{2(1-\nu_p)} \qquad (1.13)$$

where ν_p is the Poisson Ratio (0.25 ®0.30).

1.1.2.2 Radiation problems

In addition to the thermic problems, the large amount of radiation produced in the vicinity of the target constitutes one of the main difficulties of the classical positron sources. It leads to induced radioactivity in surrounding components, cooling water and air [8]. Radionuclides in the target, its metallic support (copper), the cooling water and the air are to be considered. Moreover, ozone formation increases with the beam power. Thus adequate shielding and efficient ventilation must be provided in the vicinity of the target.

1.2 Nuclear ß$^+$ decay [9]

Most of the radioactive positron sources make use of (pn) or (nγ) reactions to produce positron emitting isotopes. Suitable isotopes are listed in Table 1 and some reactions presented in Table 2. They can be created in a nuclear reactor or in a plasma. We shall take as examples:

– the production of Cu^{64} isotopes by thermal neutron capture of Cu^{63} in a nuclear reactor
– the creation of protons as projectiles in a DH_e^3 reaction in a fusion facility.

1.2.1 Cu^{64} decay

The reaction giving the desired isotope is:

$$Cu^{63} + n \Rightarrow Cu^{64} + \gamma$$

and

$$Cu^{64} \Rightarrow N_i^{64} + \beta^+ + \nu, \qquad (1.14)$$

ν being a neutrino.

The rate of positron production is given by [10]:

$$\frac{d}{dt}(n^+) = \gamma_{64} \cdot \overline{\sigma\Phi} \cdot V \cdot N \qquad (1.15)$$

Table 1
Suitable positron-emitting isotopes (from E. Ottewitte, Ref. [10])

Isotope	τ	β^+/dis	β^+	Production Reaction
Na^{22}	2.6y	0.89	0.54	Mg^{24} (d, α)
Al^{26}	$7.4x10^5$y	0.85	1.17	Mg^{24} (d, γ)
Co^{55}	18.2h	0.60	1.50,1.03,0.53,0.26	Fe^{12}(p,2n)
V^{48}	16.2d	0.56	0.69	Ti^{48}(p,n)
Ni^{57}	36h	0.50	0.85,0.72,0.35	Ni^{58} (p,pn)
Sr^{83}	33h	0.50	1.15	Sr^{84} (p,pn)
Y^{86}	14.6h	0.50	1.80,1.19	Sr^{86} (p,n)
Br^{76}	17.2h	0.44	3.57,1.7,1.1,0.8,0.6	Se^{76} (p,n)
Nb^{90}	14.6h	0.40	1.51,0.66	Zr^{90} (p,n)
Mn^{52}	5.7d	0.35	0.58	Cr^{52} (p,n)
Ge^{69}	40h	0.33	1.22,0.61,0.22	Ga^{69} (p,n)
As^{71}	62h	0.30	0.81	Ge^{72} (p,2n)
As^{72}	26h	0.30	3.34,2.50,1.84,0.67,0.27	Ge^{72} (p,n)
I^{124}	4.5d	0.30	2.20,1.50,0.70	Te^{124} (p,n)
As^{74}	17.5d	0.29	1.53,0.92	Ge^{74} (p,n)
Zr^{89}	79h	0.25	0.91	Y^{89} (p,n)
Co^{56}	77d	0.20	0.44,1.50	Fe^{56}(p,n)
Cu^{64}	12.8h	0.19	0.65	Cu^{63} (n,γ)
Rb^{84}	33d	0.17	1.63,0.82	Sr^{86} (d, α)
Co^{58}	71d	0.15	0.47	Ni^{58} (n p)

Table 2

Some (p,n) reaction producing β^+ (from J. Dawson, Ref. [11])

	$D + {}^3He \Rightarrow {}^4He + p$ (14.7 MeV)	
1.	$p + {}^{11}B \Rightarrow {}^{11}C + n$ (E_T = 2.76 MeV) ${}^{11}C \Rightarrow {}^{11}B + e^+$ ($\tau_{1/2}$ = 20 min.)	
2.	$p + {}^{13}C \Rightarrow {}^{13}N + n$ (E_T = 3 MeV) ${}^{13}N \Rightarrow {}^{13}C + e^+$ ($\tau_{1/2}$ = 10 min.)	
3.	$p + {}^{15}N \Rightarrow {}^{15}O + n$ (E_T = 3.53 MeV) ${}^{15}O \Rightarrow {}^{15}N + e^+$ ($\tau_{1/2}$ = 2.03 min.)	
4.	$p + {}^{17}O \Rightarrow {}^{17}F + n$ (E_T = 3.55 MeV) ${}^{17}F \Rightarrow {}^{17}O + e^+$ ($\tau_{1/2}$ = 66 sec.)	$\sigma \cup 200$ mb
5.	$p + {}^{18}O \Rightarrow {}^{18}F + n$ (E_T = 2.45 MeV) ${}^{18}F \Rightarrow {}^{18}O + e^+$ ($\tau_{1/2}$ = 1.87 hr.)	
6.	$p + {}^{19}F \Rightarrow {}^{19}Ne + n$ (E_T = 4.03 MeV) ${}^{19}Ne \Rightarrow {}^{19}F + e^+$ ($\tau_{1/2}$ = 18 sec.)	
7.	$p + {}^{26}Mg \Rightarrow {}^{26}Al + n$ (E_T = 5.01 MeV) ${}^{26}Al \Rightarrow {}^{26}Mg + e^+$ ($\tau_{1/2}$ = 6.5 sec.)	
8.	$p + {}^{22}N \Rightarrow {}^{22}Na + n$ ${}^{22}Na \Rightarrow {}^{22}Ne + e^+$ ($\tau_{1/2}$ = 2.6 years.)	

where γ_{64} is the β^+ branching ratio (β^+/ disintegration)

σ, the cross section for β^+ emitter production

Φ, the thermal neutron flux

V, the target volume

N, the target atom density.

Examination of this formula shows, as already pointed out by E. Ottewitte, that significant improvement can be obtained by increasing the thermal neutron flux and the target volume. The most serious limitation is that due to the rate at which heat can be removed.

1.2.2 Fusion process [11]

We can consider the reaction

$$d + He^3 \Rightarrow He^4 = p\,(14.7\text{MeV}) \tag{1.16}$$

If the plasma is seeded with B^{11} or C^{13} to produce the reactions

$$p + B^{11} \Rightarrow C^{11} + n$$
$$C^{11} \Rightarrow B^{11} + \beta^{+} + \nu,$$

we obtain a positron beam.

2. PRESENTATION OF SOME POSITRON SOURCES

We present here some typical positron sources involving electron-generated and photon-generated electromagnetic showers, together with some details of radioactive positron sources.

2.1 Electron-generated positron source

Positron sources used in present day accelerators are generated by a linac electron beam. The increasing positron yield with electron energy leads to the use of very energetic electron beams, and linear colliders are now constructed or planned with multi-GeV incident electron beams on the converter.

We already showed that positrons produced with an electron beam are emitted with a wide energy spectrum, large angles and lateral dimensions as small as those of the impinging electron beam. As new electron sources could provide small emittance beams, lateral electron beam dimensions on the target are greatly dependent on the energy spread of the electron beam. This energy dispersion leads to an enlargement of the beam dimensions in the chromatic quadrupole channel preceeding the target. Wakefields in the electron linac of the positron source give the main contribution to the energy dispersion. This induces some limitation on incident electron beam intensity. A possible scheme for an electron generated positron source is represented in Figure 10.

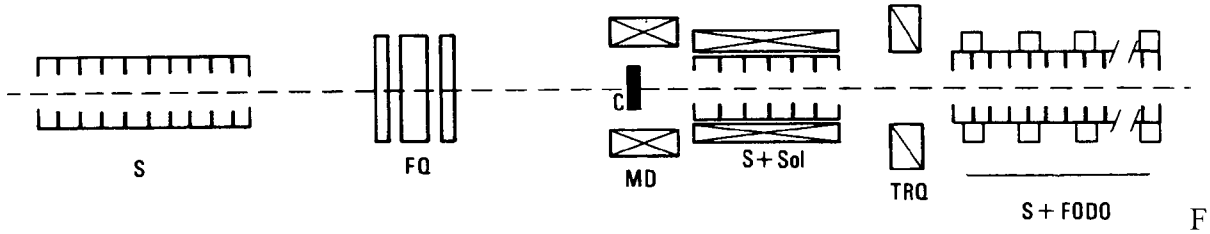

Fig. 10 Electron generated positron source

S - Accelerating section
FQ - Focusing triplet
MD - Matching device
Sol - Solenoid
TRQ - Transition optics between solenoid and FODO
C - Converter

2.2 Production of positrons using electromagnetic radiation

Instead of using very high energy electron beams on thick targets, which require a very important amount of power, we could use photons – coming for example from an undulator – to generate positrons by pair production in the target. The radiation of high energy electrons in the undulator is mainly concentrated in small angles relative to the electron velocity direction. This feature makes the method attractive for small emittance positron sources. We shall consider here two kinds of undulatory radiations for creating photons:

– in a helical undulator
– by electron channeling in a crystal.

Besides these methods, a mention is also made of a positron source using a powerful laser.

2.2.1 Production of positrons with photons from a helical undulator

Experiments using polarized particles are necessary in order to study the details of the interaction of high energy particles in the range of 100 GeV and above. This has led to serious interest in high intensity sources of polarized particles, especially positrons. One study has been initiated at Novosibirsk (Russia) for the VLEPP project [12] where the conversion system enables e^+e^- pairs, both polarized, to be obtained. The basic idea of the system is to use circularly polarized photons produced in a helical undulator by high energy non-polarized bunches of electrons coming from a linear accelerator. The main advantages of such a system are the circularly polarized photons which generate longitudinally polarized positrons, and the lower thermal effects in the converter due to the fact that the electron beam is not striking the target.

The large amount of photons and the relative low thermal effects make this solution attractive also for a source without polarization selection.

2.2.1.1 Photon and positron generation: an approach

The transverse periodic helical magnetic field of constant magnitude is produced on the axis of a double-helix-wound bifilar magnet with equal and opposite curents in each helix [13]. The orbit of the high energy electron in the helical magnetic field B is a helix having the same period, λ_W, as the field. The radius is given by:

$$b = \left(\frac{\lambda_W}{2\pi\rho}\right)^2 \rho \left[1-\left(\frac{\lambda_W}{2\pi\rho}\right)^2\right]^{-1/2} \qquad (2.1)$$

with $\rho = \gamma\beta mc^2/eB$, and where β and γ are the normalized velocity and energy.

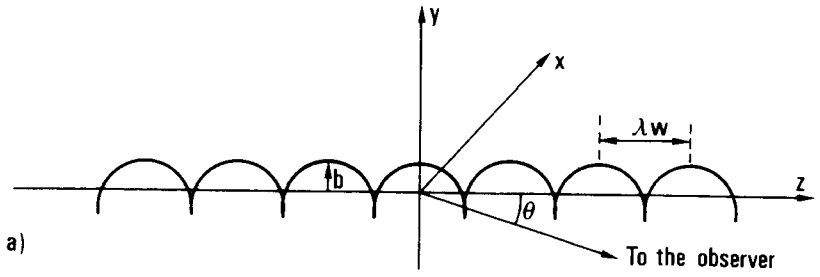

a) Physical parameters used in the text

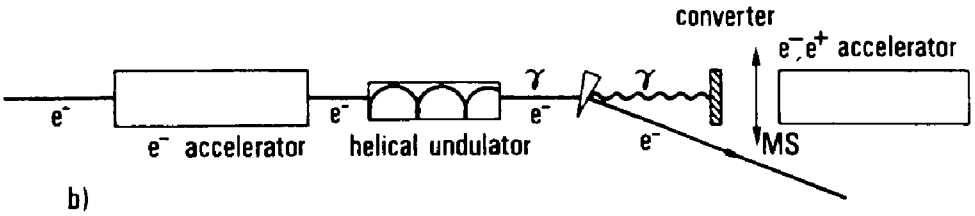

b) Lay out of a positron source using a magnetic undulator

Fig. 11 Generation of positrons with photons from a helical undulator

Synchrotron radiation is emitted in a conical angle of $\theta \sim 1/\gamma$ around the electron direction of motion (Fig. 11a). If the electron energy is very high and the number, N, of periods in the undulator very large, we have for paraxial photons a spectrum consisting of a narrow-peak at:

$$\lambda = \frac{\lambda_w}{2\gamma^2}\left(1 + K^2\right) \tag{2.2}$$

where γ is the relative electron energy,

and
$$K = \frac{\lambda_w e\, B}{2\pi\, mc} \tag{2.3}$$

The energy bandwidth is about 1/N and obviously depends on the angular divergence of the electron beam which must be restricted to:

$$\theta_{max} = \left[\gamma\sqrt{N}\right]^{-1} \tag{2.4}$$

For K = 1, we get for the peak energy of the photons:

$$E_\gamma = \frac{2\pi\hbar c\,\gamma^2}{\lambda_w}$$

For any K value, we get:

$$E_\gamma = \frac{4\pi\hbar c\,\gamma^2}{\lambda_w\left(1+K^2\right)} \tag{2.5}$$

the rate of energy loss by radiation being [14]

$$P_\gamma = \frac{2}{3}\frac{r_e c}{(mc^2)^3} E^2 F_\perp^2 \tag{2.6}$$

where E is the electron energy and $F_\perp$ = e c B.

We get for the total radiated energy of an electron:

$$\Delta w = \frac{8}{3}\pi^2 r_e\, mc^2 \frac{\gamma^2\, K^2 N}{\lambda_w} \tag{2.7}$$

So, the corresponding number of photons is [15]:

$$N_\gamma = \frac{2}{3}\pi r_e \frac{mc^2}{\hbar c} K^2\left(1+K^2\right)N$$

or

$$N_\gamma = \frac{2}{3}\pi\alpha K^2\left(1+K^2\right)N \tag{2.8}$$

where α = 1/137.

Ex : For a 100m undulator with a periodic length λ_w = 1cm, an electron of 100 GeV energy generates 250 photons of 5.3 MeV.

The positron yield is given by :

$$\eta^+ = N_\gamma \, n^+ \tag{2.9}$$

where n^+ is the number of positrons accepted by a given system expressed by:

$$n^+ = n_0 \iiint f_E(E)\, f_r(r,E)\, f_\theta(\theta,E)\, dE\, dr\, 2\pi \sin\theta\, d\theta \tag{2.10}$$

where n_0 is the total number of positrons generated by an incident photon on the target, f_E,f_θ and f_r being given by EGS simulations as in the electron generating case. The limits of integration are given by the acceptance parameters of the matching system. A scheme of the positron production using this method is given in Figure 11b.

Ex : For a 0.2 Xo thick tungsten target, 5.3 MeV photons generate positrons with a yield of 8.10^{-3} e^+/γ. We get then 2 e^+/e^- as total yield. Acceptance limitations significantly lower this value. To get higher e^+/e^- yield values one has to increase the electron beam energy and/or increase the undulator length.

2.2.1.2 Wiggler radiation based schemes

Exact calculations of photon yield and spectrum are somewhat more complicated. Actual schemes using intense wiggler radiation are under study. Linear collider projects requiring polarized positrons (VLEPP) concentrated on optimization so as to obtain a high degree of longitudinally polarized positrons. The latter depends essentially on the average circular polarization of the photons and on the energy interval of the collected positrons. Extended calculations [16, 17] showed that:

– maximum polarization must be observed near the maximum emitted positron energy,
– optimization aiming to collect a high amount of polarized photons, close to their maximal energy, leads to angular selection of the photons. A characteristic angle is then defined as: [16]

$$\gamma\theta = \frac{(1 + K^2)^{1/2}}{3}$$

which corresponds to the optimal aperture for this purpose. Wiggler parameters (B, λ_w ,N), distance between it and the target, photon collimation and converter thickness are then chosen so as to realize the required conditions.

If polarization is not required [18] wiggler length could be shorter and angular separation is less critical.

2.2.2 **Positron source generated by photons from channeled particles**

Instead of generating high energy photons by synchrotron radiation in a wiggler, we can make use of the atomic potentials in a crystal. Photon emission processes or pair creation in the crystal generated by incident particles (e^- or γ) propagating in the vicinity of the crystal axis, present different features than those of the classical interaction of incident particles with an amorphous medium, provided the angle of incidence of these particles is smaller than a critical angle:

$$\theta_c = \sqrt{\frac{2V_0}{E_0}} \tag{2.11}$$

where E_0 is the particle energy,
V_0 is the potential given by the atomic rows.

The particles undergo collective interaction with some subset of regularly situated atoms in the crystal lattice (Fig. 12).

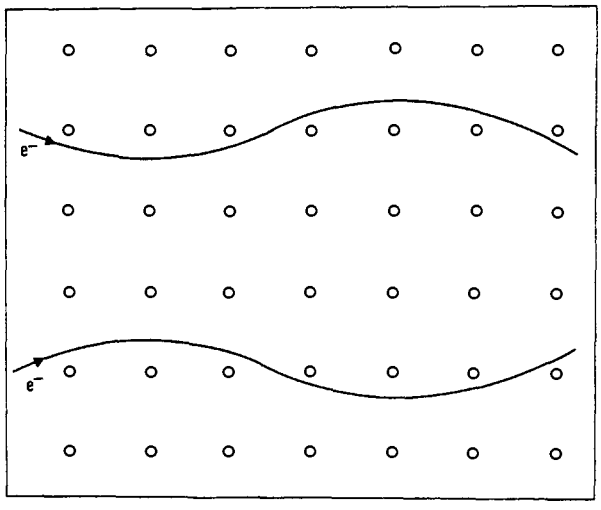

Fig. 12 Electron channeling in a crystal. This drawing is considerably exagerated. Oscillations of channeled particles occur with wavelengths of thousands of lattice spacings.

Incident particle trajectories in the crystal are very similar to those in a magnetic wiggler with a periodicity several times the atomic separation distance. This atomic wiggler presents high levels of photon production which can be used to generate positrons via pair creation in an amorphous target. However, pair creation in the crystal demands very high energy levels (more than 50 GeV) to exceed the classical Bethe-Heitler cross sections in the amorphous medium. Nevertheless, this method of producing positrons could be interesting provided that thermic and radiation effects using high intensity incident beams do not affect the crystal structure.

Extensive simulation analysis using GEANT code was undertaken aiming at a positron source associating a crystal [Si, Ge, W) to an amorphous target [19, 20]. Results showed that a large amount of soft photons – much higher than with classical Bremsstrahlung – could be created (Fig. 13). These photons are more interesting for positron production leading to yield enhancement factors close to 5 in the energy range 2-20 GeV, for targets having the same overall thickness.

A proof of principle experiment is under development at Orsay with a tungsten crystal oriented on its <111> axis and a 2 GeV electron beam [21].

Pair creation in strong fields may also be considered. Coherent pair production in crystals using high energy photon beams (E < 150 GeV) has already been measured at CERN with a germanium crystal oriented on its <110> axis. Enhancements up to 8 times the classical Bethe - Heitler (BH) cross section were found at maximum energy (150 GeV) [22]. Such results could be met at lower energies for tungsten crystals for which the energy threshold to overcome BH cross section is significantly lower than for germanium.

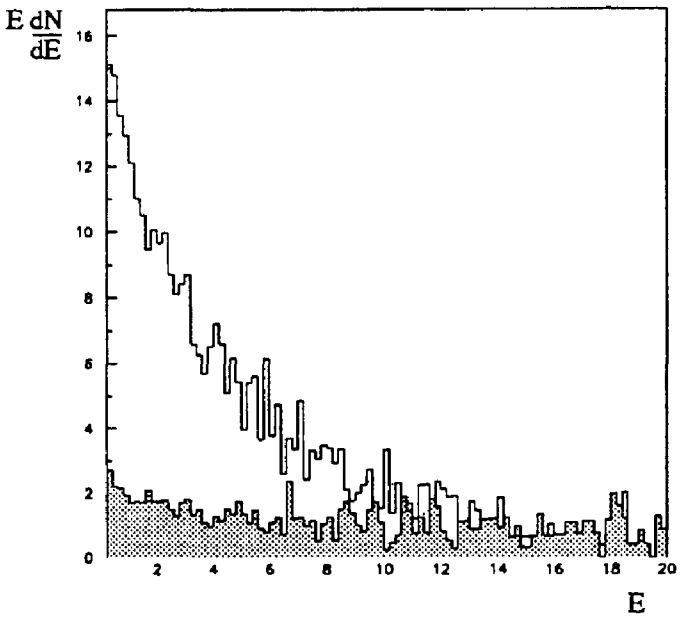

Fig. 13 Photon spectrum for incident electron energy of 20 GeV.
Tungsten on <111> axis – 1 mm thickness

2.2.3 Positron source using electron-laser interaction

A method recently proposed [23] consists of sending a powerful UV laser beam (10J ; 0.5ps) on a high energy electron beam (500 GeV). Electrons and laser light are counter moving; energetic photons and pair creation are then provided following the relations:

$$e^- + h\omega \Rightarrow e^- + \gamma$$
$$\gamma + h\omega \Rightarrow e^+ + e^-$$

The electron trajectory in the laser field-circularly polarized is a helix. Energetic photons are coming out by synchrotron radiation or Compton scattering. Positron energy could be quite large (2-3 GeV) and emittance smaller than that of the drive beam. A free-electron laser could also be foreseen to provide high power radiation.

2.3 Radioactive sources

We shall take as an example of a radioactive source that designed for the BNL experiment [10] which uses the Cu^{64} decay. In this case the rate of positron production (Eq. (1.15)) is :

$$\frac{d}{dt}\left(n^+\right) = \underbrace{0.19}_{\beta^+} \times \underbrace{3.6 \times 10^{-24} \times 8 \times 10^{14}}_{\overline{\sigma_{63}\phi}} \times \underbrace{\frac{1}{16}}_{V} \times \underbrace{0.075 \times 10^{24}}_{N} \times \underbrace{0.8}_{\text{after some irradiation period}}$$

i.e. ,

$$\frac{d}{dt}\left(n^+\right) = 2.1 \times 10^{12}\ e^+/s.$$

Higher e^+ fluxes have been obtained by test reactors e.g. INEL/ATR (Idaho National Engineering Laboratory, US Navy) with more than 10^{17} e^+/s. These reactors require large irradiation volumes to perform multi-magnitude increase in positron production. Thus, the INEL/ATR has nine large channels presenting a total irradiation volume of 2.6×10^4 cm^3: such a facility allows more than a factor of 5 in magnitude improvement of the positron production.

As mentioned before, e^+ rate improvement using larger source volumes poses two difficult problem :

– how to transform from a large, voluminous positron source into a compact beam
– increasing the volume may lead to self absorption, so a limitation on thickness exists.

3. POSITRON COLLECTION: THE MATCHING SYSTEM

The characteristic emittance of the positron source at the converter – large angles, small lateral dimensions – has to be transformed into small angles, large lateral dimensions, so as to fit with the accelerator acceptance. The choice of the matching device is therefore dependent on:

– the expected positron yield
– the allowed energy dispersion.

Two kinds of matching devices are now mainly used on positron accelerators:

– narrow-band systems such as the quarter-wave transformer
– large-band systems such as the adiabatic device.

Other kinds of matching devices such as the lithium and plasma lens may also be used.

3.1 Matching devices using a solenoidal magnetic field [4, 24]

3.1.1 The solenoidal magnetic field

Due to the cylindrical symmetry of the solenoid about the z axis, the only non-zero component of the potential vector $\vec{A}$ in cylindrical coordinates (r, ø, z) is:

$$A_ø = \frac{r}{2} B(z) - \frac{1}{16} r^3 \frac{d^2B}{dz^2} \tag{3.1}$$

The Lagrangian,

$$L = - m_0c^2 \sqrt{1 - v^2 / c^2} - \left(V - \vec{A}.\vec{v}\right)$$

may be expressed in these coordinates as;

$$L = - m_0c^2 \sqrt{1 - \frac{\left(r^2 + r^2 \phi^2 + z^2\right)}{c^2}} - e\left(V - r^2\phi \frac{B}{2}\right). \tag{3.2}$$

Conjugate variables (q, p) are defined by:

$$p = \frac{\partial L}{\partial \dot{q}} \cdot \tag{3.3}$$

We can therefore observe that the absence of ϕ in the expression of L gives

$$p_\phi = \text{constant}$$

which expresses the invariance of the angular momentum.

The transport matrix of the solenoid can be represented in the following way. The Lagrange equation:

$$\frac{d}{dt} \cdot \frac{\partial L}{\partial \dot{q}_j} - \frac{\partial L}{\partial q} = 0 \tag{3.4}$$

gives with cartesian coordinates:

$$\frac{d}{dz}\left(P \frac{dx}{dz} - \frac{eB}{2} y\right) = \frac{eB}{2} \frac{dy}{dz}$$

$$\text{and } \frac{d}{dz}\left(P \frac{dy}{dz} + \frac{eB}{2} x\right) = -\frac{eB}{2} \frac{dx}{dz} \tag{3.5}$$

where P represents the scalar momentum.

A convenient way to handle the particle dynamics in a solenoidal magnetic field is to transform these coordinates into ones (ξ, η) with a rotation angle given by the Larmor angle

$$\chi = \int_0^z \frac{eB}{2P}\, dz. \tag{3.6}$$

Such a transformation is represented by:

$$\begin{pmatrix} \xi \\ p_\xi \\ \eta \\ p_\eta \end{pmatrix} = \begin{pmatrix} \cos\chi & 0 & -\sin\chi & 0 \\ 0 & \cos\chi & 0 & -\sin\chi \\ \sin\chi & 0 & \cos\chi & 0 \\ 0 & \sin\chi & 0 & \cos\chi \end{pmatrix} \begin{pmatrix} x \\ p_x \\ y \\ p_y \end{pmatrix} \tag{3.7}$$

The equations of motion are then:

$$p'_\xi = \frac{d}{dz}\left(P\xi'\right) = -\left(\frac{eB}{2}\right)^2 \cdot \frac{\xi}{P}$$

$$p'_\eta = \frac{d}{dz}(P\eta') = -\left(\frac{eB}{2}\right)^2 \cdot \frac{\eta}{P} \cdot \tag{3.8}$$

Motions for ξ and η are decoupled and can be handled separately. The equations (3.8) may be written:

$$\begin{aligned} \xi'' + \frac{P'}{P}\xi' + \left(\frac{eB}{2P}\right)^2 \xi = 0 \\ \eta'' + \frac{P'}{P}\eta' + \left(\frac{eB}{2P}\right)^2 \eta = 0 \end{aligned} \tag{3.9}$$

For a constant field B, and in the absence of an accelerating field, these equations are those of a classical harmonic oscillator of constant frequency eB/2P. The transformation matrix is then, in the (ξ, p_ξ) plane for example,

$$\begin{pmatrix} \xi \\ p_\xi \end{pmatrix} = \begin{pmatrix} \cos\chi & \frac{2}{eB}\sin\chi \\ -\frac{eB}{2}\sin\chi & \cos\chi \end{pmatrix} \begin{pmatrix} \xi_0 \\ p_{\xi 0} \end{pmatrix} \tag{3.10}$$

We can associate with the variables (ξ, p_ξ) and $(\eta\ p_\eta)$, the Hamiltonians:

$$\begin{aligned} H_1 = \frac{eBc}{4P}\left[\frac{eB}{2}\xi^2 + \frac{2}{eB}p_\xi^2\right] \\ H_2 = \frac{eBc}{4P}\left[\frac{eB}{2}\eta^2 + \frac{2}{eB}p_\eta^2\right] \end{aligned} \tag{3.11}$$

If we define a frequency $\omega = \dfrac{ebc}{4\pi P}$, the quantity:

$$\frac{H}{\omega} = \pi\left[\frac{eB}{2}\xi^2 + \frac{2}{eB}p_\xi^2\right] \tag{3.12}$$

is an adiabatic invariant of the motion. So, we can write:

$$\left(\frac{eB}{2}\right)^2(\xi^2 + \eta^2) + (p_\xi^2 + p_\eta^2) = \text{constant}$$

Coming back to the variables $[x\ p_x\ ;\ y\ p_y]$, we may writ :

$$\left(\frac{eB}{2}\right)^2(x^2 + y^2) + (p_x^2 + p_y^2) = \text{constant} \tag{3.13}$$

This relation holds everywhere in the solenoid. It represents the equation of a hyperellipsoid in the phase space $[x\ p_x\ ;\ y\ p_y]$. The volume comprised in this hyperellipsoid is constant [Liouville Theorem].

3.1.2 Narrow-band system: The quarter-wave transformer (QWT)

This system is widely used in positron accelerators. It is made from a short lens with a high magnetic field and a long solenoidal magnetic field extending over several accelerating sections [25]. Such a field profile is represented in Figure 14. The most recent versions of this device use a short pulsed lens with a high magnetic field just after the converter in the vacuum chamber (DESY [26], Frascati [27], LEP [28], KEK [29].

We can associate with the transport matrix of the system – which is symplectic – a quadratic form:

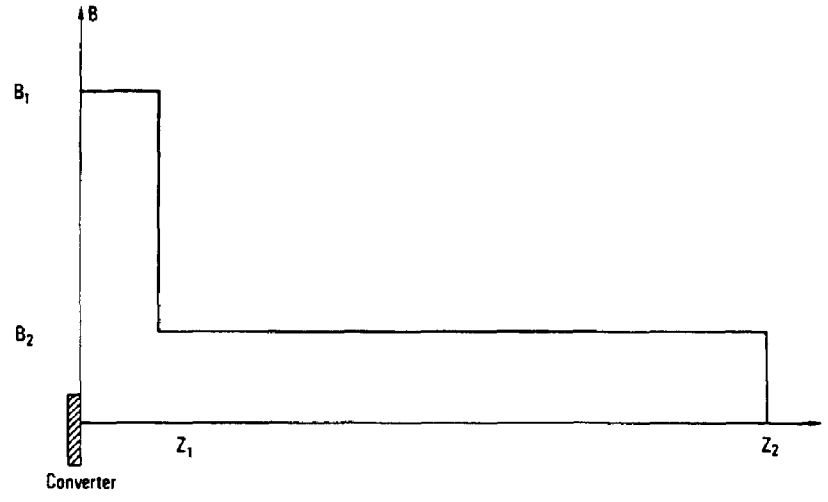

Fig. 14 Field profile of the quarter-wave transformer

$$XX^* + \left(\frac{2}{eB_2}\right)^2 P_x P_x^* = \left(\cos^2\chi_1 + \left(\frac{B_1}{B_2}\right)^2 \sin^2\chi_1\right) X_0 X_0^*$$

$$+ \left[\left(\frac{2}{eB_1}\right)^2 \sin^2\chi_1 + \left(\frac{2}{eB_2}\right)^2 \cos^2\chi_1\right] P_{x_0} P_{x_0}^* \qquad (3.14)$$

$$+ \frac{2}{eB_1} \sin\chi_1 \cos\chi_1 \left[1 - \left(\frac{B_1}{B_2}\right)^2\right] (X_0^* P_{x_0} + X_0 P_{x_0}^*)$$

where $X = x + iy$, $P_X = p_x + ip_y$

X^* and P_x^* are the conjugate values,

χ_1 represents the Larmor angle followed by the particle in the first lens.

We may observe that:

$$\left(\frac{e\,B_2}{2}\right)^2 XX^* + P_X P_X^* = \left(\frac{e\,B_2}{2}\right)^2 (x^2 + y^2) + (p_x^2 + p_y^2) = C \qquad (3.15)$$

C being a constant.

A positron emitted on the converter with a scalar momentum P_0 and phase space coordinates X_0 and P_{X_0} can be transmitted at the end of the (long) solenoid only if:

$$XX^* \leq a^2 \tag{3.16}$$

where a represents the iris radius of the accelerating cavities. This condition implies:

$$C - \left(\frac{2}{eB_2}\right)^2 P_X P_X^* \leq a^2$$

or in cylindrical coordinates,

$$C - \left(\frac{2}{eB_2}\right)^2 \left[p_r^2 + \frac{p_\phi^2}{r^2}\right] \leq a^2$$

which gives the value of

$$C = a^2 + \left(\frac{2}{eB_2}\right)^2 . \frac{p_\phi^2}{a^2} . \tag{3.17}$$

The set of points in the phase space which satisfy the condition (3.16) constitutes the acceptance volume of the system.

We may write, using the cylindrical coordinates (r, ϕ, p_r, p_ϕ), and for $\chi_1 = \frac{\pi}{2'}$ the quadratic form corresponding to the acceptance figure:

$$\left(\frac{B_1}{B_2}\right)^2 . \left(\frac{r_0}{a}\right)^2 + \left(\frac{p_{r_0}}{\frac{eB_1 a}{2}}\right)^2 + \left(\frac{p_{\phi_0}}{\frac{eB_1 a^2}{2}}\right)^2 \left[\frac{1}{\left(\frac{r_0}{a}\right)^2} - \frac{1}{\left(\frac{B_2}{B_1}\right)^2}\right] = 1. \tag{3.18}$$

We may define [30]

$$\frac{r_0}{a} = \rho, \qquad \frac{p_{r_0}}{\frac{eB_1 a}{2}} = \zeta, \qquad \frac{p_{\phi_0}}{\frac{eB_1 a^2}{2}} = \Phi$$

Equation (3.18) then becomes:

$$\left(\frac{B_1}{B_2}\right)^2 \rho^2 + \zeta^2 + \Phi^2 \left[\frac{1 - \left(\frac{B_1}{B_2}\right)^2 \rho^2}{\rho^2}\right] = 1. \tag{3.19}$$

Integration of the volume comprised in the hyperellipsoid gives:

$$V = 2\pi^2 \left(\frac{eB_1 a^2}{2}\right)^2 \int_0^{\rho max} \sqrt{1 - \left(\frac{B_1}{B_1}\right)^2 \rho^2}\ \rho\ d\rho. \tag{3.20}$$

However, integration is feasible only if:

$$\rho = \frac{r_0}{a} \leq \frac{B_2}{B_1} . \tag{3.21}$$

This condition defines the radial acceptance of the system. Then, we obtain:

$$V = \frac{2\pi^2}{3}\left(\frac{eB_2a^2}{2}\right)^2 \tag{3.22}$$

Therefore, the acceptance volume expression of the quarter-wave transformer calculated for $\chi_1 = \pi/2'$, i.e. for particles with a half helical period in the short lens, has a close dependence on the radius of the iris as well as on the strength of the solenoid magnetic field.

The total acceptance of the system is obtained if we evaluate the contributions from the particles emitted at the converter in the whole energy spectrum, i.e for any χ_1. In this case, the hyperellipsoid equation is given by [4]:

$$\left[\cos^2\chi_1 + \left(\frac{B_1}{B_2}\right)^2 \sin^2\chi_1\right] r_0^2 + \left[\left(\frac{2}{eB_1}\right)^2 \sin^2\chi_1 + \left(\frac{2}{eB_2}\right)^2 \cos^2\chi_1\right]\left(p_{r_0}^2 + \frac{p_{\phi_0}^2}{r_0^2}\right)$$

$$+ \frac{4}{eB_1} \sin\chi_1 \cos\chi_1 \left[1 - \left(\frac{B_1}{B_2}\right)^2\right] r_0\, p_{r_0} = a^2 + \left(\frac{2}{eB_2}\right)^2 \frac{p_{\phi_0}^2}{a^2} \tag{3.23}$$

Integration of the volume comprised in the acceptance hyperellipsoid gives:

$$V(\chi_1) = \frac{2\pi^2}{3}\left(\frac{eB_2a^2}{2}\right)^2 \left[1 - \left(1 - \frac{1}{\sin^2\chi_1 + \left(\frac{B_1}{B_2}\right)^2 \cos^2\chi_1}\right)^{3/2}\right] . \tag{3.24}$$

Figure 15 represents this acceptance volume for a quarter-wave transformer defined by:

B_1 = 20 kgauss
B_2 = 4 kgauss
L = 4.7 cm (short lens length)

The angular acceptance in each plane may be calculated by observing that the maximum p_x or p_y value at the converter plane is $\frac{eB_1}{2}a$. Since:

$$p_x = Px' + e\,A_x$$

and

$$x_0\,(p_{x\,max}) = 0$$

and

$$y_0\,(p_{x\,max}) = r_0 = \textbf{Error!}.\ a$$

we get :

$$\theta_{max} = x'_{max} = \frac{eB_1\,a}{2P}\left[1 + \frac{B_2}{B_1}\right]. \qquad (3.25)$$

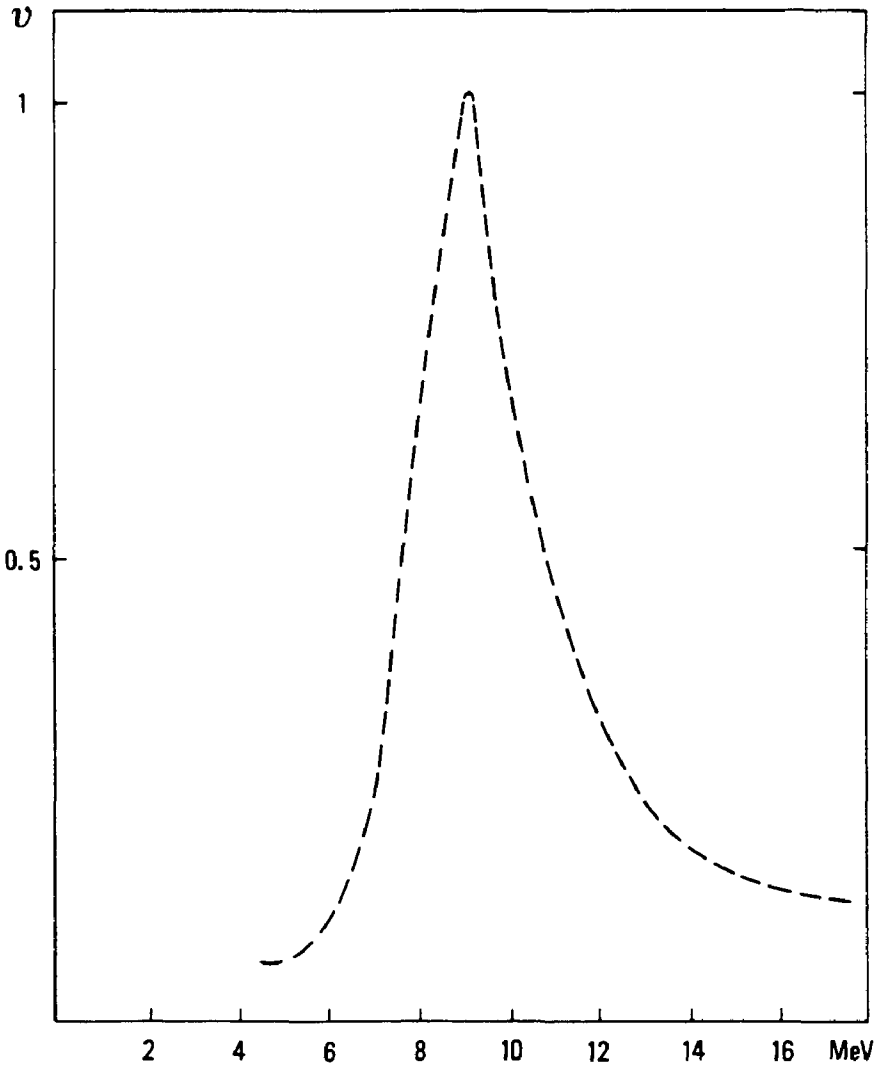

Fig. 15 Acceptance volume for a QWT

A convenient representation of the phase space is given by the intersection of the hyperellipsoid with the plane ($y_0 = 0$; $p_{y0} = 0$) as shown in Figure 16.

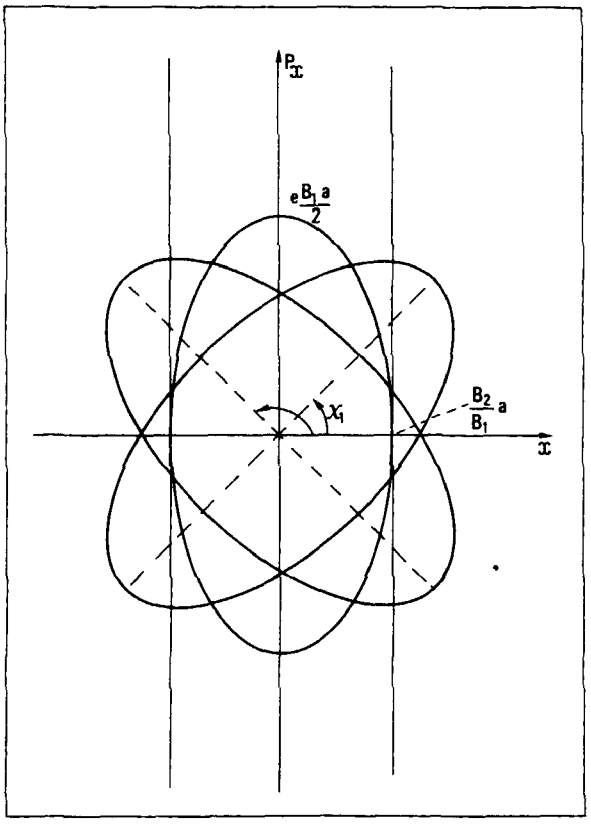

Fig. 16 Intersection of the hyperellipsoid with the plane ($y_0 = 0$; $p_{y0} = 0$) for the QWT

3.1.3 Large-band system : The adiabatic device (AD)

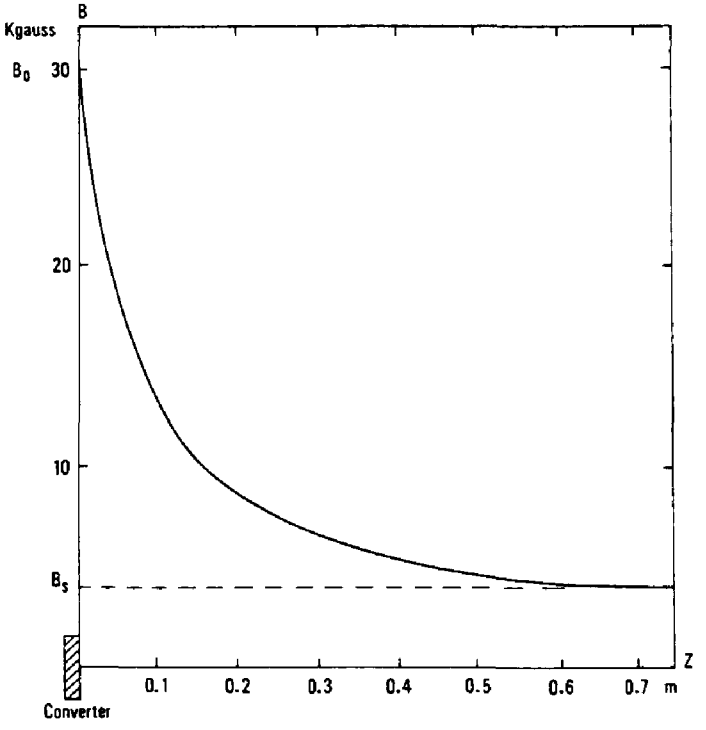

Fig. 17 Field profile of the adiabatic device

This system used at SLAC [31] and Orsay [32] is made of a slowly varying magnetic field lens followed by a long solenoidal magnetic field extending over some accelerating sections. Between the maximum (B_0) and the minimum (B_S) values, the magnetic field adiabatically tapers (see Figure 17) so as to conserve the adiabatic invariant:

$$\oint_i p_i \, dq_i = \frac{\pi p_\perp^2}{eB} \tag{3.26}$$

where (q_i, p_i) are the conjugate variables
$p_\perp$ the transverse momentum and,
B the field strength.

If the magnetic field changes slowly, so does the period of the motion and the adiabatic invariant $J = A/\pi$. The parameter of smallness ε of this variation must be very weak. So:

$$\varepsilon = \frac{P}{eB^2} \cdot \frac{dB}{dz} \ll 1. \tag{3.27}$$

Transport matrix

With a slowly varying magnetic field, Eq. (3.9) may be integrated using the WKBJ Method [33] and under the assumption (3.27), we obtain the expression of the transport matrix in the rotating frame.

$$\begin{pmatrix} \xi \\ p_\xi \end{pmatrix} = \begin{pmatrix} \left[\frac{B_0}{B}\right]^{1/2} \cos\phi & \frac{2}{e[B_0 B]^{1/2}} \sin\phi \\ -\frac{e[B_0 B]^{1/2}}{2} & \left[\frac{B}{B_0}\right]^{1/2} \cos\phi \end{pmatrix} \begin{pmatrix} \xi \\ p_{\xi_0} \end{pmatrix}. \tag{3.28}$$

The adiabatic magnetic field varies along z following:

$$B(z) = \frac{B_0}{1 + \mu z} \tag{3.29}$$

where $\mu = \dfrac{\varepsilon B_0}{P_0}$

ε, the parameter of smallness and
P_0 a particular (central value) of the scalar momentum for the emitted positron. As before, a quadratic form may be worked out using the transport matrix (symplectic) of the whole system.

Acceptance considerations

The quadratic form is given by:

$$XX^* + \left(\frac{2}{eB_S}\right)^2 P_X P_X^* = \left[\frac{B_0}{B_S}\right] X_0 X_0^* + \frac{4}{e^2[B_0 B_S]} P_{X_0} P_{X_0}^* = \text{constant}. \tag{3.30}$$

Applying the condition (3.16), we get for the acceptance hyperellipsoid:

$$\left[\frac{B_0}{B_s}\right]\left(\frac{r_0}{a}\right)^2 + \left(\frac{p_{r_0}}{\frac{e\sqrt{B_0 B_s}\,a}{2}}\right)^2 + \left(\frac{p_{\phi_0}}{\frac{eB_s a^2}{2}}\right)^2\left[\frac{B_s}{B_0}\cdot\frac{1}{\left(\frac{r_0}{a}\right)^2} - 1\right] = 1. \tag{3.31}$$

Integration of the phase-space volume comprised in the hyperellipsoid gives the acceptance volume:

$$\mathcal{U} = 2\pi^2 \frac{B_0}{B_s}\left(\frac{eB_s a^2}{2}\right)^2 \int_0^{\rho_{max}} \sqrt{1 - \frac{B_0}{B_s}\rho^2}\;\rho\, d\rho. \tag{3.32}$$

Under the assumption

$$\rho = \frac{r_0}{a} \le \sqrt{\frac{B_s}{B_0}} \tag{3.33}$$

which constitutes the radial acceptance condition for the adiabatic system, we get:

$$\mathcal{U} = \frac{2\pi^2}{3}\left(\frac{eB_s a^2}{2}\right)^2. \tag{3.34}$$

This acceptance volume is calculated regardless of the positron energies.

The positron energy does not appear in the hyperellipsoid equation as it did for the quarter wave transformer. The adiabatic system presents a very large energy acceptance. However, all these results have been calculated with the condition (3.27) fulfilled whereas for a given field law, not all the particles obey this condition. In particular, the high energy positrons make the parameter ε too big and, a high energy limitation exists.

The angular acceptance may be calculated as previously for the QWT. We get:

$$\theta_{max} = \frac{e\sqrt{B_0 B_s}}{P}\cdot a \tag{3.35}$$

As before, we show in Figure 18 the intersection of the phase-space volume with the plane ($y_0 = 0$; $p_{y0} = 0$).

3.1.4 Comparaison between AD and QWT devices

It is worth remarking that a comparison between the two systems may be made assuming $B_1 = B_0$ and $B_2 = B_s$. We then notice that:

– Radial acceptance is larger in the adiabatic case
– Angular acceptance is larger in the QWT case
– Energy acceptance is much larger in the adiabatic case.

These different features make the Adiabatic device more interesting for high energy positron linacs (multigev for example) where the relative energy spread ΔE/E can be held at a reasonable level. Moreover, the permissible source diameter at the converter being larger by a factor $\sqrt{B_0/B_s}$ the thermal constraints are less stringent.

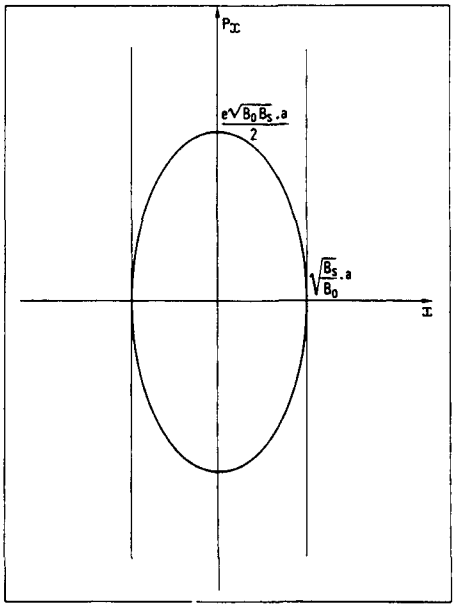

Fig. 18 Intersection of the hyperellipsoid with the plane ($y_0 = o$; $py_o = o$) for the adiabatic matching system

3.2 Matching devices using an azimuthal magnetic field

An azimuthal magnetic field created by a longitudinal current circulating in the same direction of the particles could provide a strong focusing. If Ro is the radial dimension of the "wire" such a field is defined by:

$$\begin{cases} B = \left(\frac{\mu_0 I}{2\pi R_0^2}\right) r & \text{for } r < R_0 \\ B = \frac{\mu_0 I}{2\pi r} & \text{for } r > R_0 \end{cases}$$

where I is the circulating current and r the radial displacement of the particle. A sketch of the magnetic field is given below (Figure 19).

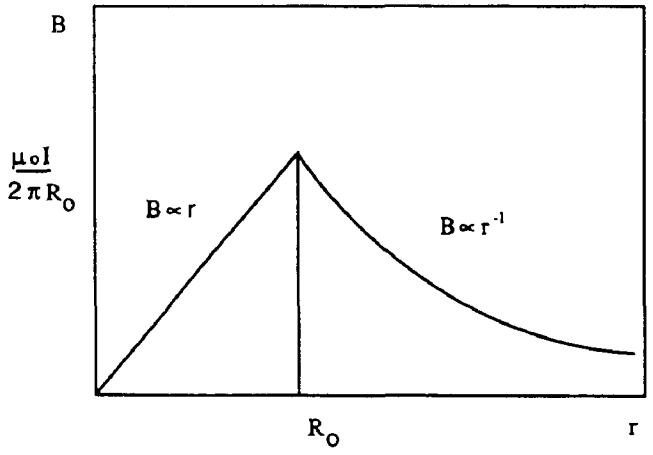

Fig. 19 Sketch of the azimuthal magnetic field

This field focuses one kind of particle (e^+) and defocuses the other (e^-) making beam control easier in the following part of the accelerator. Two kinds of devices have been elaborated using this principle : lithium lenses (LL) and plasma lenses (PL). Both have been tested for antiproton focusing and one of them (PL) for ion focusing.

3.2.1 Lithium lenses

This lens is made of a cylindrical lithium conductor fed with a unipolar current pulse. As mentioned before, the field is linearly dependent on the radial distance from the axis in the whole conductor. Typical dimensions are 10 cm length and a few mm diameter. Pulsed currents may exceed 100 kA for peak value [34]. For such a lens, a minimum value for Ro is desirable to minimize the excitation current. A limitation is put however on radius minimization due to skin depth; uniform current distribution requires a large δ while heating limitations lead to decreasing δ. A compromise is often taken so as to balance current uniformity and resistive heating [34]. This lens has been used at Novosibirsk, FERMILAB and CERN, and is optimized to focus low energy particles (some MeV) while presenting a fairly good acceptance angle ($\alpha > 0.5$ rad). The multiple scattering angle is about 50 mrad at 20 MeV and very high intensity currents produce magnetic fields of several Tesla [35].

3.2.2 Plasma lenses

If we look at a non-absorbing medium with an azimuthal magnetic field created by a longitudinal current, the plama lens could give an interesting opportunity with high magnetic fields. In the plasma lens based on the Z-pinch effect, the conductor is a column of ionized gas – hydrogen for example. A high intensity pulsed current created with an appropriate discharge circuit and flowing through the ionized gas produces an imploding plasma column. The positrons moving through the plasma when the "pinch" is reached, are strongly focused by the azimuthal magnetic field. Such a device has been studied in many laboratories and especially at CERN for the antiproton source of the ACOL project.

Experiments done at CERN (p, $\bar{p}$) [36] and at GSI-Darmstadt (Heavy ions) [37] showed successful results. Beam size reduction as high as 40 were obtained (GSI). A possible configuration for a plasma lens dedicated to positron collection has been examined [38]. The converter may be used as the anode of the device. Field gradients exceeding 30 T/m are required to fulfil focusing conditions for a LIL type positron source. Such values are already reachable.

3.2.3 Comparison of lithium and plasma lenses

Experiments developed on ACOL led to comparisons between the two kinds of lenses. Similar collected antiproton yields were obtained with both devices [36]. Differences between them were related mainly to the nature of the medium:

- smaller amount of matter (PL) led to less scattering and absorption of the secondary particles.
- induced radioactivity, after a cumulated number of 10^{16} protons have been delivered to the target, presented ten times less value (PL) than with a lithium lens [36].

Important technological efforts are under development for both lenses.

3.3 Phase slippage in the matching system

Phase slippage makes some contribution to positron beam energy spread. At some distance from the converter, we can write for the positron beam energy dispersion:

$$\Delta E^{+} = \left[\Delta E_s^2 + \Delta E_\phi^2\right]^{1/2}$$

where ΔE_S is the energy dispersion at the converter i.e. the accepted energy spread. ΔE_ϕ is the contribution of phase slippage to energy dispersion and arises from the difference in velocities of the accepted positrons, and from the path-length differences of trajectories in the magnetic fields.

3.3.1 Phase slippage due to difference in velocities

The phase slippage is given by

$$\Delta\phi_v = \frac{\pi}{\lambda_{RF}} \cdot \int_0^L \left(\frac{1}{\gamma^2} - \frac{1}{\Gamma^2}\right) dZ \tag{3.36}$$

where λ_{RF} is the RF wavelength;

Γ is the reference particle energy in units of $m_o c^2$.

3.3.2 Phase slippage due to path-length differences

The path-length differences occur in the matching device and constant field solenoid. So, we can write for the QWT [39]:

$$\Delta\phi_\ell = \frac{2\pi}{\lambda_{RF}} \cdot \frac{a^2}{\gamma_c \lambda_2}\left[\frac{\pi}{4} \cdot \frac{\lambda_2}{\Lambda_1}\left(1 + \frac{\lambda_2^2}{\Lambda_1^2}\right) + \frac{2}{\alpha\lambda_2}\right] \tag{3.37}$$

where

$$\lambda_2 = \frac{2\ m_0 c}{eB_2}, \qquad \Lambda_1 = \frac{2\ m_0 c}{eB_1}$$

γ_c is the central energy in units of $m_o c^2$ (energy corresponding to half helical period followed in the short lens),

α is the accelerating gradient.

For the adiabatic device, we can also write:

$$\Delta\phi_\ell = \frac{2\pi}{\lambda_{RF}} \cdot \frac{a^2}{\gamma_c \lambda_s}\left[\frac{1}{\varepsilon}\log\frac{\lambda_s}{\Lambda_0} + \frac{2}{\alpha\lambda_s}\right]$$

where ε is the parameter of smallness.

$$\lambda_s = \frac{2\ m_0 c}{eB_s}, \qquad \Lambda_0 = \frac{2\ m_0 c}{eB_0}$$

The energy dispersion due to phase slippage is roughly given by : $\frac{\Delta E}{E} \# \frac{1}{8}(\Delta\phi)^2$.

4. EMITTANCE TRANSFORMATION AND PRESERVATION

The solenoidal magnet system which is used after the matching system requires high power. A quadrupole focusing system is generally inserted some distance after the solenoid, typically when positrons have an energy of about 100 MeV. The transition between solenoidal and quadrupoles focusing is made as soon as the spacing between the quadrupoles allows this. The quadrupoles are thus put on the accelerating sections with a FODO sequence. A matching device is generally inserted between the solenoid and the quadrupole systems to transform the axisymmetric beam coming from the solenoid into the well known elliptical shape of the FODO system. The positron beam transverse emittance is quite large, 2 to 5 MeV/c mm or,

$$\varepsilon_n = 4.10^{-3} \quad \text{to} \quad 10^{-2} \quad \text{mm mrad.}$$

This emittance has to be reduced before the interaction point in damping rings (DR) producing synchrotron radiation. Damping and excitation due to quantized emission of photons provide an equilibrium beam size which is smaller than that entering the DR.

Since the required positron bunch length is usually shorter than that delivered by the DR, bunch length compression, has to be applied. This is done in a two-stage process:

- acceleration of the bunch in a RF cavity: the phase of the bunch centre is at 0 so as to accelerate the particles ahead of this point and decelerate those behind
- non isochronous transport of the bunch: the higher energy particles travel on a longer path than those of lower energy.

As a result, all the positrons arrive at the linac entrance at almost the same time so that the bunch length is shortened while the energy spread is increased.

Geometrical misalignments in a linac cause perturbations of the beam trajectory. Since the positron beam emittance before damping is relatively large, accurate steering to avoid beam losses in the accelerating sections is required. Trajectory perturbations can be caused by quadrupole misalignments (displacements and rotation of the quadrupole axis), accelerating-section misalignments and gradient errors. Analytical evaluations have shown that the lateral quadrupole displacement is the most critical misalignment while tilt around one of their transverse axes is the effect next in importance. Trajectory control using beam-position monitors associated with steering dipoles allows the beam lateral displacements to be minimized and hence prevents significant wake field perturbations for high intensity positron beams [40].

5. COMPARISON OF POSITRON SOURCES

A comparison of positron sources – existing or starting – is presented in Table 3. The two parameters associated with the incident electron beam, peak intensity I^- or number of electrons per bunch N^- and energy E^-, are represented by their values at the converter location. Target material and matching device are also indicated. The two magnetic field values represent (B_1, B_2) and (B_0 B_s) for the quarter-wave transformer and the adiabatic device respectively. Positron yield normalized to 1 GeV incident electron beam is reported for three corresponding measurements:

– as close as possible to the target (total yield)
– at the linac output
– in the beam switchyard ; slit width is indicated in % of the final energy.

Emittance measurements are also reported.

Some remarks can be inferred from this table:

1) Normalized positron yield values are mostly between 2 and 4 x 10^{-2} e^+/e^- for total accelerated particles.

2) The useful yield – in a given energy slit – is roughly half of the Linac output yield for a 1 % energy bandwith. For the SLC this useful yield is obviously very close to the linac output yield due to the high final energy.

3) Undamped positron emittances scale from π to more than 4π mm mrad for a 1 GeV positron beam. Discrepancies are quite important between the measurements. Different acceptance features of the positron linacs do not completely explain that. The very small emittance of the SLC positron beam – two orders of magnitude lower than the others – is obviously due to the damping ring.

Table 3
Positron sources compared

Facilities	e^-		e^+ source		e^+/e^- GeV^{-1}			Emittance mm. mrad
	I^- (A) or (N^-)	E^- (GeV)	Target	Matching	Total yield	Linac output	Beam switch.	
LEP (LIL) CERN	2.5	0.2	W	QWT 18-3 kgauss		2.5.10-2	1.5.10^{-2} (Δ%)	6π (500 MeV)
DESY (Hambourg)	1.4	0.28	W	QWT 20-3 kgauss		4.10^{-2}	2.4.10^{-2} ($\angle$0. 5%)	13π (360 MeV)
KEK (Tsukuba)	10	0.25	Tantalum	QWT 23-4 kgauss	6.5.10-2	1.8.10-2 2.5 GeV		12π 250 MeV)
LAL (Orsay)	0.8	1	W	AD 12.5-1.8 kgauss	3.10^{-2}	2.10^{-2}	10^{-2} ($\angle$0. 5%)	2π (1GeV)
SLC (Stanford)	3 x 10^{10}	33	W-26 Re	AD 50-5 kgauss	8.10^{-2}		2.10^{-2} (IP)	3π x 10^{-4} (50 GeV)

6. SUMMARY AND CONCLUSIONS

Quantitative results on positron production using shower codes are available and allow precise determination of the expected number of positrons. These results can be compared to the measurements carried out on existing positron sources. Reliable matching systems working in many laboratories give the possibility of choosing the device most adapted to the problem.

If we consider a positron source devoted to a linear collider, we notice that the required maximization of the luminosity induces some stringent conditions on positron beams. The requirements concern intense bunches for positrons as for electrons, very small emittances and a high repetition rate. The small emittance constitutes an attainable goal as shown by the SLC experience using damping rings. However, the large number of particles per bunch – from 10^{10} to 10^{12} – and the high repetition frequency seem somewhat difficult to handle if one requires a high number of impinging electrons on the positron target to produce the required bunch population.

Since beam intensity is limited by wakefield effects, one cannot increase the intensities of the positron beam by simply increasing the electron beam intensity well above the positron

intensity needed. So we are led to a yield of 1 e^+/e^-, at least concerning the accepted positrons. Moreover, thermic and radiation problems in the target limit the incident electron power. If the interest associated with high energy electron beams is clearly demonstrated, one has to consider the effects of a large number of particles impinging on a small area of the target. Rotating targets could be a solution.

Semi-classical methods using photons instead of electrons on amorphous targets may offer attractive alternatives for future e^+ sources while radioactive sources, though offering the possibility of large number of e^+ as in the test reactors, present too many difficulties.

Positron sources generated by photons from undulators are nowadays under intense analysis and considered in almost half of the linear collider projects as the desirable issue for the positron source. More recent ideas are under consideration (laser) or under theoretical and experimental investigation (channeling).

* * *

REFERENCES

[1] B. Rossi, High energy particles, Prentice Hall, Ed. (1956)

[2] W.R. Nelson, R.L Ford, The EGS code system, SLAC 210 (1978)

[3] A. Crawford, M. Messel, Electron-photon shower distribution function tables for lead, copper and air absorbers, Pergamon Press, Oxford (1970)

[4] R. Chehab, Etude de la production et du confinement d'un faisceau de positrons. Application à l'Accélérateur Linéaire d'Orsay, RI/75-4 (Avril 75)

[5] R. Brun et al, GEANT 3, CERN - DD/EE 84 - 1

[6] H. De Staebler, More calculations for positron target test in ESA, Internal memo CN–24 (Avril 1980)

[7] S. Ecklund, Positrons for linear colliders, SLAC Pub 4484 (Nov. 87)

[8] P. Sievers, M. Höfert, Radiological problems at high energy, high intensity electron-positron converters, CLIC note 71 (July 1988)

[9] K.G. Lynn, W.E. Frieze, Intense positron beams and possible experiments in "Positron scattering in Gases", J. Humberton & M.R. McDowell Ed., Nato ASI Series

[10] E. Ottewitte, Large scale positron production for physics needs via fission reactors, Proc. of the Advanced Accelerator concepts Conference, Madison, WI 1986

[11] J. Dawson, A positron factory. Proceedings of the Workshop "Critical issues in the development of new linear colliders", Madison, Wisconsin (August 1986)

[12] V. Balakin, A. Mikhailichenko, The conversion system for obtaining highly polarized electrons and positrons, Preprint INP 79 - 85 Novosibirsk

[13] B. Kincaid, Journal of Applied Physics Vol. 48, n 7 (July 1977)

[14] M. Sands, in "Physics with intersecting storage rings" (1971) Academic Press, B. Toushek, Ed.

[15] H. Wiedemann, SLAC Pub 2849 (November 1981)

[16] E.G. Bessonov, A.A. Mikhailichenko, Some aspects of undulator radiation forming for conversion system of the linear accelerator, Preprint Budker INP 92-43

[17] A.D. Bukin, A.A. Mikhailichenko, Optimized target strategy for polarized electrons and positrons production for linear colliders, Preprint Budker INP 92-76

[18] K. Flottman, J. Rossbach, A high intensity positron source for linear collider, DESY M-91-11, October 91

[19] R. Chehab et al, Proc. of IEEE Particle Accelerator Conference, Chicago, IL, March 20-23, 1989

[20] X. Artru et al, Proc. of IEEE Particle Accelerator Conference, San-Francisco, CA, May 6-9, 1991

[21] R. Chehab, Proc.of the Linear Collider 92 Workshop, July 92, Garmisch

[22] A. Belkacem et al, Nucl. Instr. & Meth. B13 (1986) 9

[23] P. Chen, R. Palmer, Positron production by electron-laser interaction, Proc. of the Linear Collider 92 Workshop, July 92, Garmisch

[24] R. Helm et al, The positron source in "The Stanford Two Mile Accelerator", R. Neal Editor, W.A. Benjamin Inc (1968).

[25] J. Haïssinski, Nucl. Instr. & Meth. 51 (1967) 181.

[26] G. Stange, IEEE Trans. Nucl. Science, NS-26 n 3 (June 1979)

[27] R. Boni, S. Guiducci, M. Vescovi, A new system for positron focusing at the Frascati Linac, LNF-81/6 (R) (1981)

[28] R. Belbeoch et al., Rapport d'études sur le projet des linacs injecteurs de LEP (LIL), LAL PI 82-01/T, LAL Orsay

[29] A. Enomoto and al, Proc. of the 1986 Linac Conference, Stanford (June 1986)

[30] R. Helm, SLAC - 4, Stanford Linear Accelerator Center, Stanford (August 1962)

[31] F. Bulos et al, IEEE Transactions on Nuclear Science, NS-32 n 5 (October 1985) also: J.E. Clendenin et al, SLAC Pub 4704 (September 1988)

[32] R. Chehab et al, IEEE Transactions on Nuclear Science, NS-30 n 4 (August 1983)

[33] J. Heading, An introduction to Phase Integral Methods, London: Methuen, New York: John Wiley (1962)

[34] B.F. Bayanov et al, Nucl. Instr. & Meth. 190 (1981)9

[35] G.I. Silvestrov Problems of intense secondary particle beam production, Preprint INP 86-163 Novosibirsk (1986)

[36] R. Kowalewicz et al, Performance of the CERN plasma lens in laboratory and beam tests at the antiproton source, Proc. 1991 IEEE PAC, San-Francisco, May 91

[37] E. Boggasch et al, Plasma lens fine focusing of heavy ion beams, Appl. Phys. Letters 60 (20) 1992, p. 2475

[38] H. Braun et al, Application of plasma lenses in positron sources, Proc. of the 1992 EPAC, Berlin, March, 1992

[39] F. Amman, Positron accelerators in "Linear Accelerators", P. Lapostolle, A. Septier Editors, North-Holland Pub. Co (1970)

[40] R. Chehab, Y. Thiery, K. Hübner, Proc. of the 1986 Linear Accelerator Conference, June 1986, Stanford.